Biomedicine & Pharmacotherapy 187 (2025) 118074

Contents lists available at ScienceDirect

Biomedicine & Pharmacotherapy

journal homepage: www.elsevier.com/locate/biopha

A novel noninvasive test based on near-infrared fluorescent cholephilic probes for hepatobiliary secretory function assessment

Beatriz Sanchez de Blas [a,b,1], Alvaro G. Temprano [a,b,1], Candela Cives-Losada [a,b], Oscar Briz [a,b], Elisa Lozano [a,b], Maria L. Martinez-Chantar [b,c], Matias A. Avila [b,d], Mattia Mori [e], Ahmed Ghallab [f,g], Jan G. Hengstler [f], Concepción Perez-Melero [h], Francisco A. Bermejo-Gonzalez [i], Maria J. Monte [a,b], Marta R. Romero [a,b,2], Jose J.G. Marin [a,b,*,2]

[a] Experimental Hepatology and Drug Targeting (HEVEPHARM), University of Salamanca, IBSAL, Salamanca, Spain
[b] Center for the Study of Liver and Gastrointestinal Diseases (CIBEREHD), Carlos III National Institute of Health, Madrid, Spain
[c] Liver Disease Laboratory, Center for Cooperative Research in Biosciences (CICbioGUNE), Basque Research and Technology Alliance (BRTA), Derio, Spain
[d] Hepatology Laboratory, Solid Tumors Program, Center for Applied Medical Research (CIMA), University of Navarra, Pamplona, Spain
[e] Department of Biotechnology, Chemistry and Pharmacy, University of Siena, Siena, Italy
[f] Department of Toxicology, Leibniz Research Centre for Working Environment and Human Factors (IfADo), Technical University of Dortmund, Germany
[g] Department of Forensic Medicine and Toxicology, Faculty of Veterinary Medicine, South Valley University, Qena, Egypt
[h] Pharmaceutical Chemistry Laboratory, Pharmaceutical Sciences Department, University of Salamanca, IBSAL, Salamanca, Spain
[i] Organic Chemistry, School of Chemistry, University of Salamanca, Salamanca, Spain

ARTICLE INFO

Keywords:
Bile acid
Bile secretion
Cholestasis
NIRBAD
Transport

ABSTRACT

Routine serum biomarkers do not always accurately reflect impaired liver function. To overcome this limitation, we synthesized novel bile acid (BA) derivatives (NIRBADs) with near-infrared (NIR) fluorescence that can penetrate the abdominal wall and be detected extracorporeally. NIRBAD dynamics in the liver parenchyma were recorded through intravital imaging in mice and extracorporeally in both rats and mice. NIRBAD metabolism was analyzed using HPLC-MS/MS and fluorimetry. Transport was investigated in cells expressing BA transporters, whose interactions with NIRBADs were assessed through molecular docking and dynamics simulations. The hepatic NIRBAD clearance time (NCT) was evaluated in animal models with impaired secretory function: rats with hepatocellular cholestatic damage induced by phalloidin and mice with obstructive cholestasis caused by bile duct ligation (BDL), as well as with spontaneous development of sclerosing cholangitis (*Mdr2*$^{-/-}$). NIRBADs were taken up by cells expressing NTCP or OATP1B3, but minimally by OATP1B1. These findings were consistent with the NIRBAD dynamics in the liver parenchyma and *in silico* studies. Following intravenous administration of a non-toxic dose, the time course of NIR fluorescence in the rat liver aligned with biliary output. In mice with BDL, hepatic NIR fluorescence remained stable throughout the experimental period. Phalloidin administration impaired rat bile flow, induced a decrease in biliary NIRBAD-1 output, and caused an increase in NCT. Furthermore, the NCT was significantly longer in *Mdr2*$^{-/-}$ than in wild-type mice. In conclusion, a novel, noninvasive, real-time test based on cholephilic probes with NIR fluorescence detectable extracorporeally serves as a valuable tool for assessing hepatobiliary secretory function.

Abbreviations: BA, bile acid; BDL, bile duct ligation; CA, cholic acid; CHO-K1, Chinese hamster ovary cells; CGamF, cholyl-glycyl-amido fluorescein; DCA, deoxycholic acid; ICG, indocyanine green; ICG-FC, indocyanine green dye fluorescence cholangiography; NCT, NIRBAD clearance time; NIR, near-infrared radiation; NIRBAD, near-infrared fluorescent bile acid derivative; NTCP, Na^+-taurocholate co-transporting polypeptide; OATP, organic anion transporting polypeptide; TCA, taurocholic acid.

* Correspondence to: Department of Physiology and Pharmacology, University of Salamanca, Campus Miguel de Unamuno, E.D.-231, Salamanca 37007, Spain.
E-mail address: jjgmarin@usal.es (J.J.G. Marin).

[1] Both authors share the first authorship of this work.
[2] Both authors contributed equally as senior authors of this work.

https://doi.org/10.1016/j.biopha.2025.118074
Received 22 November 2024; Received in revised form 3 March 2025; Accepted 17 April 2025
Available online 28 April 2025

1. Introduction

The limited repertoire of molecules available for studying liver function [1] includes bile acid (BA) derivatives, for instance, labeled with radioactive isotopes, such as [^{14}C], [^{3}H], and [^{18}F], or tagged with fluorochromes [2,3]. Their usefulness has been restricted to investigations using *in vitro* and *in vivo* laboratory models. Conversely, methods such as MRI with gadoxetate and cholescintigraphy with iminodiacetic acid derivatives and metastable technetium-99 [^{99m}Tc] have been employed to diagnose hepatobiliary disorders [4]. Nevertheless, these radiopharmaceuticals are not cholephilic compounds and thus lack hepatobiliary selectivity [5]. The emergence of new innocuous and noninvasive techniques for hepatobiliary imaging, such as those based on near-infrared (NIR) fluorescence, broadens the range of probes available for investigation and diagnosis. NIR light can efficiently penetrate living tissues due to its greater scattering than absorption characteristics. Therefore, NIR spectroscopy can serve as a valuable technology for diagnosis, as it provides real-time insights into various physiological and pathological processes in tissues and organs [6]. The NIR spectrum, with an emission wavelength of 700–1000 nm, serves as a crucial analytical tool across various fields, including the food, chemical, biochemical, environmental, pharmaceutical, and medical industries [7]. NIR technology depends on the absorption of specific chromophores across various wavelengths, allowing a consistent-intensity light beam to selectively filter wavelengths passing through tissue, which aids in detecting particular chromophores. Therefore, the availability of a contrast agent within this radiation band, compatible with existing imaging techniques for diagnosing hepatobiliary pathologies, would be beneficial in the clinical setting [8]. Since the initial application of indocyanine green (ICG) for angiography in the 1970s, significant progress has been made in NIR imaging for mapping blood vessels and refining surgical procedures. ICG has been used in real-time imaging to assist in the intraoperative identification of malignant nodules during oncological surgeries like liver resection and clinical exploration in hepatocellular carcinoma (HCC), thereby enhancing the likelihood of complete tumor resection [9] and hence

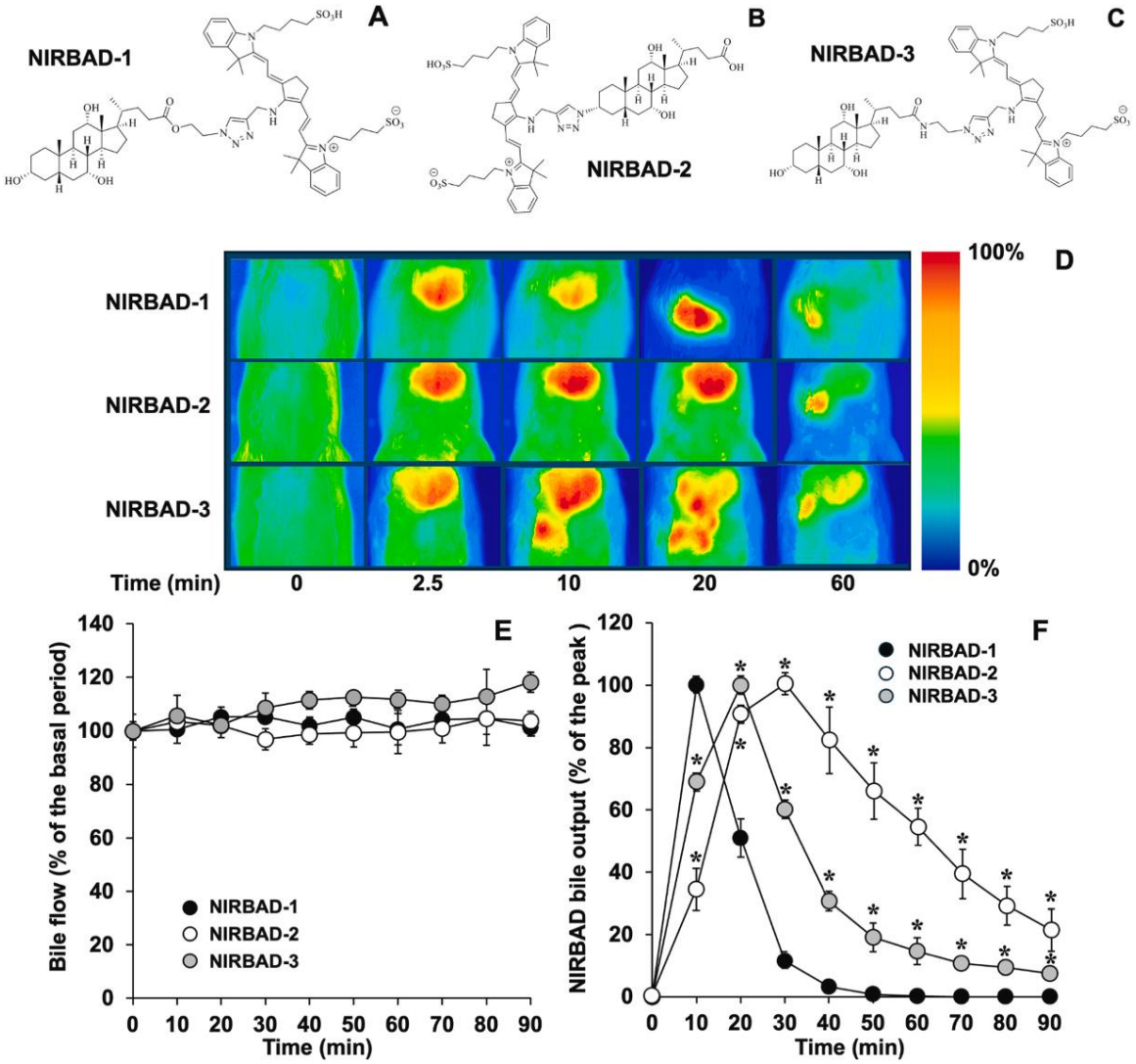

Fig. 1. Structure of the near-infrared bile acid derivatives NIRBAD-1 (A), NIRBAD-2 (B), and NIRBAD-3 (C). Extracorporeal near-infrared fluorescence was detected in the abdominal area after intravenous administration of NIRBADs (1 μmol) to anesthetized rats without surgical manipulation (D). Bile flow (E) and fluorescence bile output (F) were measured following NIRBADs administration in rats with a catheter implanted in the common bile duct. Bile flow is expressed as a percentage of the average value determined during the 20-min basal period in each animal before NIRBADs administration. No significant differences ($p > 0.05$) among them or during the experimental period (90 min) were found. Values for fluorescence output into bile are expressed as a percentage of the highest data point during the experiment for each case. Values are presented as mean±SEM. * : $p < 0.05$; compared to NIRBAD-1. In all groups $n \geq 5$. Excitation wavelength was 710 nm, whereas fluorescence was recorded using a 785–900 nm LP filter.

mitigating postoperative complications [10]. Moreover, ICG-associated NIR fluorescence has been proposed to evaluate liver function after tumor resection and hepatectomy [11] because it can be helpful in detecting postoperative malfunction [12] and potentially metastatic liver tumors with greater sensitivity than radioisotope-based methods [13]. Ongoing investigations have explored various applications of ICG, including its utility in cholangiography (ICG-FC) [14]. The main limitation of ICG is its absence of organ selectivity.

In this field, we pioneered the development of novel liver-vectorized probes. Thus bile acid derivatives capable of emitting NIR fluorescence (NIRBADs), whose molecular structures are illustrated in Fig. 1A-C, were synthesized. The reaction substrates and products, along with the synthesis methods, chemical-physical characterization, chemical stability, and photostability, have been previously published [15]. In this study, we have investigated the cholephilic characteristics of these compounds. The results provide a proof of concept for the usefulness of NIRBADs as a tool for real-time, non-invasive hepatobiliary function assessment. The prospect of translating this technology into clinical practice is appealing due to the safety of NIR fluorescence. Furthermore, the ability to detect probes from outside the body without surgical intervention minimizes patient discomfort and reduces background noise.

2. Methods

2.1. Chemicals

Taurocholic acid (TCA), rhodamine 123, rifampicin, and phalloidin were purchased from Sigma-Aldrich (Merck, Madrid, Spain), while alkynocyanine 718 (CAS: 1188292–54–7) was obtained from LuminoChem Ltd. (Budapest, Hungary). They were acquired with a purity exceeding 98 %, as indicated by the suppliers. Cholyl-glycyl-amido fluorescein (CGamF), NIRBAD-1, NIRBAD-2, and NIRBAD-3 were synthesized following previously described methods and published protocols [15,16]. More precisely, NIRBADs were obtained by conjugating cholic acid (CA) with alkynocyanine 718 at the carboxylic group via ester or amide spacers or at the -OH group at the 3α-position through a triazole linkage [15]. All other reagents were of analytical grade.

2.2. Cell culture

The Chinese ovarian hamster cell line CHO-K1 (ATCC CCL-61) was purchased from the American Type Culture Collection (LGC Standards, Barcelona, Spain). Monoclonal cells expressing the human transporters Na^+-taurocholate cotransporting polypeptide (NTCP) or organic anion transporting polypeptide 1B3 (OATP1B3) were generated by transduction with recombinant lentiviral vectors (pWPI) introduced into target cells at an appropriate multiplicity of infection (MOI 25), which was facilitated by hexadimethrine bromide (Polybrene, Merck), as described previously [17]. Transduced cells were maintained for at least four days before selecting clonal stably expressing cells using the limiting dilution method. Clones exhibiting the highest efficacy for the uptake of CGamF a fluorescent BA derivative that is substrate of the these transporters [17,18], were selected for further investigation. CHO-K1 cells stably transfected with human organic anion transporting polypeptide 1B1 (OATP1B1) [19] were provided by Peter Meier, Bruno Hagenbuch and Bruno Stieger (University of Zurich, Switzerland). Cells were cultured at 37°C in a 5 % CO_2 atmosphere with 80 % relative humidity and maintained in DMEM High Glucose medium supplemented with 0.43 mM L-proline (Merck, Madrid, Spain), 1 % GlutaMAX® solution, 10 % heat-inactivated (56°C for 30 min) fetal bovine serum, and 1 % penicillin-streptomycin-amphotericin B (Fisher Scientific). CHO cells stably transfected with OATP1B1 were also cultured in this medium containing 400 μg/ml G418 and, during the last 24 hours before the experiments, were supplemented with 5 mM sodium butyrate to enhance transporter expression. To ensure that there was no mycoplasma contamination in the cultures, periodic PCR tests were performed using a Mycoplasma Biotools kit (B&M Labs, Madrid, Spain).

2.3. Transport studies

For *in vitro* studies, CHO-K1 cells - either wild-type (WT) or transduced with pWPI empty vectors (Mock), which served as control groups - were compared with cells stably expressing NTCP (CHO-NTCP), OATP1B1 (CHO-OATP1B1), or OATP1B3 (CHO-OATP1B3), all of which were cultured using established protocols [20]. To assess drug uptake, experiments were conducted using 3–5 distinct cultures for each data point. Subconfluent cells were trypsinized, resuspended in uptake medium (96 mM NaCl, 0.8 mM $MgSO_4$, 5.3 mM KCl, 1.1 mM KH_2PO_4, 1.8 mM $CaCl_2$, 11 mM *D*-glucose, and 10 mM HEPES/Tris, pH 7.4) and subsequently incubated in the presence of 10 μM NIRBADs, with or without 100 μM of inhibitors (TCA or rifampicin, as appropriate), at 37°C for 15 min. Uptake was stopped by washing the cells with ice-cold buffer, followed by measurement of intracellular fluorescence using a flow cytometer (FACSCalibur, Becton Dickinson, Madrid), with appropriate excitation (laser source of 488 nm wavelength) and emission (560 nm filter of LP cutoff) conditions, based on previous studies [15].

2.4. In silico studies

The 3D structures of the OATP1B3 extracellular and transmembrane domains were generated by homology modeling utilizing the Prime-2.1 software [21]. The human OATP1B3 coding sequence was obtained from the Uniprot database [22,23] under accession code Q9NPD5. Molecular docking simulations were performed using GOLD version 5.6.3, with the ChemScore scoring function [24] to optimize docking accuracy. The best binding pose for each compound was selected based on the scoring results. Molecular dynamics (MD) simulations were carried out using Amber18, with the ff14SB41 force field [25] applied for protein parameterization. The General Amber Force Field (GAFF) [26] was used to parameterize BAs. All the procedures and intermediate results are described in detail in Supplementary Fig. 3–8.

2.5. Animal models

Male Wistar rats (220–250 g) and male *Mdr2*$^{-/-}$ mice (≈25 g) (FVB.129P2-Abcb4^{tm1Bor}/*J*, Jackson Laboratory, USA) along with their wild-type littermates (≈25 g) were used in this study. Previously described procedures were performed to generate models of acute cholestasis. Extrahepatic obstructive cholestasis by common bile duct ligation and sectioning (BDL) [27] or hepatocellular cholestasis by phalloidin administration [28] were performed just before functional tests. Animal procedures received approval from the University of Salamanca Ethical Committee for Laboratory Animals, following Spanish and European guidelines, and in accordance with the NIH Guide for the Care and Use of Laboratory Animals. The animals were kept under controlled environmental conditions with a temperature of 20°C and a 12 h/12 h light/dark cycle. They had *ad libitum* access to water and standard rodent chow (Panlab, Madrid, Spain). All experiments were performed under suitable anesthesia, using either pentobarbital (in rats, 50 mg/kg b.wt., i.p., Nembutal N.R.; Abbott, Madrid) or isoflurane (in mice, Forane®; Abbott Madrid). At the end of the experiments, anesthetic overdose with pentobarbital was used for euthanasia of rats, while euthanasia of mice was performed by exsanguination under anesthesia of the animal with isoflurane.

2.6. Real-time monitoring in vivo extracorporeal fluorescence

NIRBADs, or alkynocyanine 718 (1 μmol in rats or 200 nmol in mice), were dissolved in DMSO and diluted to 12 % in saline solution before being intravenously administered to anesthetized animals. Extracorporeal fluorescence in the upper abdominal area was monitored using a highly sensitive (3.2 MP) CCD camera (Luminescent Image Analyzer

LAS-4000 imaging system; Fujifilm Life Science, Madrid). Excitation was achieved with an LED lamp at a wavelength of 710 nm, and fluorescence was recorded using a 785–900 nm LP filter. Multi Gauge V3.0 software was used for the analysis of the images.

2.7. Bile secretion in anaesthetized rats

A median laparotomy was performed on anesthetized rats to implant a catheter into the common bile duct, allowing for the collection of bile in 10-min intervals throughout the experiments, as previously described [28]. Intravenous administration of NIRBADs or phalloidin was carried out according to protocols and methods outlined elsewhere [28]. Upon completion of the experimental period, a blood sample was obtained from the cava vein to determine serum parameters through routine biochemical analysis, and the livers were excised and weighed. Bile fluorescence due to the secretion of NIRBADs and their metabolites was measured using a spectrofluorometer (Hitachi F-4500, Triad Scientific, 514 Manasquan, New Jersey). The excitation and emission wavelengths were set at the maximum values for each compound, as previously reported [15].

2.8. Functional intravital imaging

Functional intravital imaging of NIRBAD flux in the livers of anesthetized C57Bl6/N mice was performed using a confocal microscope (LSM880, Zeiss, Germany), as previously described [29]. Before recording, the mice received bolus tail vein injections of rhodamine 123 (ThermoFisher Scientific; excitation wavelength 488 nm), which is a marker of mitochondrial membrane potential and lobular zonation [30]. NIRBADs were administered intravenously using a mouse catheter fixed in the tail vein. The dyes were first dissolved in DMSO at 20 mM stock concentrations and further diluted 1:20 in phosphate-buffered saline directly before injection into mice (50 µL per mouse). The excitation and emission maximum of all NIRBADs occurred at 633 nm and 678 nm wavelengths, respectively.

2.9. Biochemical analyses of serum markers

Serum markers of hepatic and renal toxicity were analyzed using appropriate test strips (Spotchem II Liver-1 and Spotchem II Kidney-3, Arkray Factory, A. Menarini Diagnostics, Badalona, Spain) read in an automatic dry chemistry analyzer (Spotchem EZ SP-4430). Serum levels of aspartate aminotransferase (GOT or AST, IU/dl), alanine aminotransferase (GPT or ALT, IU/dl), albumin (Alb, g/dl), total bilirubin (T-Bil, mg/dl), total protein (T-Pro, g/dl), blood urea nitrogen (BUN, mg/dl), uric acid (UA, mg/dl), and creatinine (Cre, mg/dl) were measured.

2.10. HPLC-MS/MS analyses

NIRBADs and their metabolites were detected in bile by HPLC-MS/MS (6420 Triple Quad LC/MS, Agilent Technologies, Santa Clara, CA, USA). Chromatographic separation was performed with gradient elution using a Zorbax Eclipse XDB-C18 column (150 mm × 4.6 mm, 5 µm) maintained at 35°C. The flow rate was 500 µl/min, and the initial mobile phase was 73:27 methanol/water (both containing 5 mM ammonium acetate and 0.01 % formic acid, pH 4.6), which was changed to 93:7 methanol/water over 10 min and then returned to 73:27 in 1 min. Electrospray ionization (ESI) in positive mode was used under the following conditions: gas temperature 350°C, gas flow 11 ml/min, nebulizer 45 psi, capillary voltage 2500 V. Acquisition was first performed in scan mode to identify those peaks appearing in bile after NIRBADs administration, as compared to those found in basal bile. The identity of NIRBADs was then confirmed in multiple reaction monitoring (MRM) mode, using the specific m/z transitions 606–579 and 411 for NIRBAD-1, 583.7–565.7 and 281.2 for NIRBAD-2, and 605–578 and 281 for NIRBAD-3. The bile samples were diluted with methanol and centrifuged (13,000 rpm, 5 min) before HPLC injection.

2.11. Statistical analyses

Statistical analyses, including paired or unpaired Student's *t*-tests, were applied as appropriate to assess the significance of differences among groups. Differences were regarded as statistically significant at $p < 0.05$. Microsoft Excel (version 15.32) and GraphPad (Prism5) were utilized for these analyses.

3. Results

3.1. Cholephilic characteristics of NIRBADs in rats

The rationale for designing NIRBADs was to obtain cholephilic fluorescent probes, which were investigated in two different models using anesthetized rats. In intact animals receiving intravenous administration of NIRBADs, NIR fluorescence was detected in the abdominal area extracorporeally, first in the liver and later in the intestine (Fig. 1D, Supplementary Video 1). In the second group of rats, a catheter was placed into the common bile duct by laparotomy to record bile flow (Fig. 1E) and biliary fluorescence output (Fig. 1F). None of the administered compounds affected bile flow, which was relatively steady during the experimental period (Fig. 1E). This was consistent with the lack of acute toxicity, which was determined at the end of this time by measuring serum markers of liver and kidney injury (Supplementary Table 1). The time course of fluorescent compound output into bile (Fig. 1F) revealed that the fluorescence peak in bile after NIRBAD-1 administration rapidly reached its maximum and subsequently decreased to undetectable levels before 60 min. In contrast, NIRBAD-2-associated fluorescence took longer to reach a maximum, and its output in bile was still incomplete 90 min after administration (Fig. 1F). The fluorescence in the bile after NIRBAD-3 administration followed an intermediate pattern (Fig. 1F).

3.2. Dynamics of NIRBADs in mouse liver parenchyma

Intravital imaging was performed to study the dynamics of NIRBADs in the liver parenchyma (Fig. 2). First, the liver tissue was visualized by being preloaded with rhodamine 123 and perfused with fluorochrome. After NIRBADs were administered, fluorescence was initially detected in the sinusoids, which interacted with the basal plasma membrane of hepatocytes.

In the case of NIRBAD-1, fluorescence accumulated in the intracellular space of hepatocytes and was rapidly secreted into bile (Supplementary Videos 2a and 2b). Fluorescence in the canaliculi was clearly seen when the intracellular signal was fading, before vanishing from the parenchyma a few minutes later. Images taken at a longer time (45 min) revealed the absence of NIRBAD-1 in the liver parenchyma (Fig. 3A).

The fluorescence due to NIRBAD-2 accumulated in the hepatocytes and was subsequently transferred to both the canaliculi and back to the basolateral membrane (Supplementary Videos 3a and 3b). Fluorescence in the parenchyma persisted longer than in the case of NIRBAD-1. Images at min 45 showed an intense signal due to NIRBAD-2, which was mainly located in the pericentral zone of the liver acini (Fig. 3B). NIRBAD-3 dynamics showed an intermediate pattern. NIRBAD-3-associated fluorescence in the canaliculi was as evident as in the case of NIRBAD-1, but, like NIRBAD-2, it was also detected returning to the basolateral membrane (Supplementary Videos 4a and 4b). The disappearance of NIRBAD-3-associated fluorescence from the liver parenchyma was faster than that of NIRBAD-2 but slower than that of NIRBAD-1 (Fig. 2). At min 45, although the periportal zones of the liver parenchyma had already eliminated NIRBAD-3, fluorescence remained in the pericentral regions (Fig. 3C).

Supplementary material related to this article can be found online at doi:10.1016/j.biopha.2025.118074.

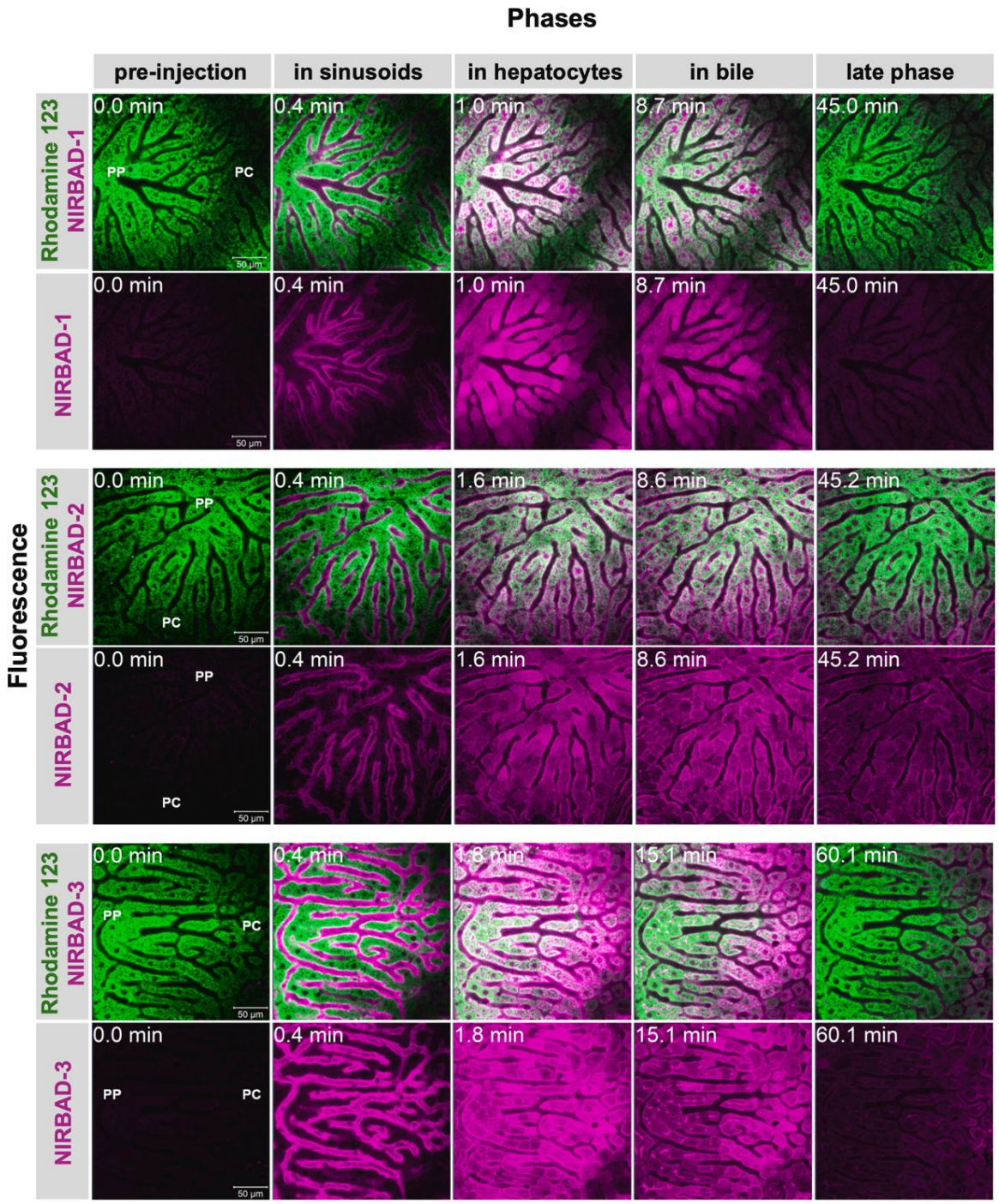

Fig. 2. Time course of intravital confocal microscopy visualization showing the intrahepatic uptake and temporal distribution in the liver parenchyma of NIRBAD-1, NIRBAD-2, and NIRBAD-3 (pink fluorescence) after intravenous administration (50 nmol) in mice. Rhodamine 123 was used as a probe to visualize the parenchyma (green fluorescence). PP, periportal region; PC, pericentral region. The excitation and emission maximum of all NIRBADs occurred at 633 nm and 678 nm wavelengths, respectively.

3.3. Intrahepatic metabolism of the probes

Chromatographic analysis of rat bile after NIRBAD-1 administration revealed that although a few minor peaks were detected by UV absorbance in bile collected at the maximum value of fluorescence (Fig. 4A), only two major peaks (#1 and #2) were confirmed to be due to fluorescent compounds, accounting for signals of similar magnitude of fluorescence (Fig. 4B). Mass spectrometry of these two peaks showed *m/z* signals that were absent in fractions collected from the chromatographic separation of basal bile (Fig. 4C and Fig. 4E) but appeared in peaks #1 (Fig. 4D) or #2 (Fig. 4F). These *m/z* signals were consistent with a compound released from NIRBAD-1 that contained part of the fluorochrome of this molecule in the case of peak #1 (inset of Fig. 4D) and unaltered NIRBAD-1 in the case of peak #2 (inset of Fig. 4F). In the case of NIRBAD-2 (Supplementary Fig. 1) and NIRBAD-3 (Supplementary Fig. 2), two fluorescence peaks were detected. However, in both cases, one of the peaks was markedly higher than the other. Mass spectrometry analysis revealed that the most intense fluorescent peak in the bile after NIRBAD-2 or NIRBAD-3 administration was due to the unaltered BA derivative.

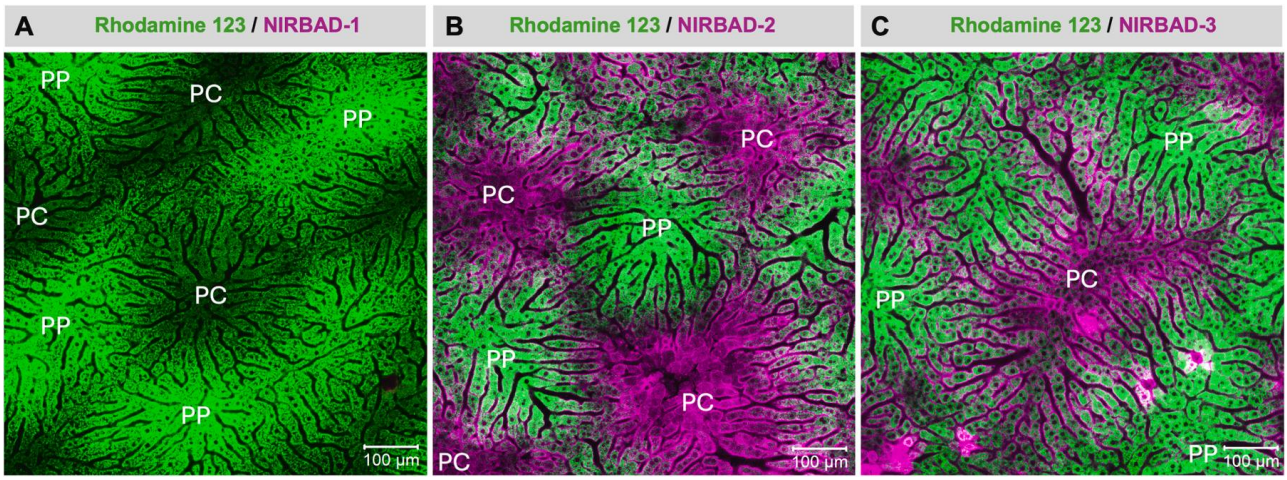

Fig. 3. Representative pictures of intravital confocal microscopy visualization showing the remaining fluorescence in mouse liver 45 min after i.v. administration of 50 nmol NIRBAD-1 (A), NIRBAD-2 (B), and NIRBAD-3 (C) (pink signal). Rhodamine 123 was used as a probe to visualize the parenchyma (green signal). PP, periportal region; PC, pericentral region. No pink signal was detected in panel A. The excitation and emission maximum of all NIRBADs occurred at 633 nm and 678 nm wavelengths, respectively.

3.4. Fixing a new in vivo functional test

Real-time evolution of NIR fluorescence in the rat liver (Fig. 5A) revealed that NIRBAD-1 was rapidly taken up by this organ, reaching maximal values of extracorporeal fluorescence at 2.4 ± 0.4 min. This loading step was followed by a relatively short clearance phase (~ 20 min). The unconjugated fluorescent moiety (alkynocyanine 718) was taken up by the rat liver more slowly and persisted in this organ at approximately 80 % of the maximal signal for at least 90 min. NIRBAD-2 was taken up at a slower rate than NIRBAD-1 (maximal liver load was reached at min 17.4 ± 3.3), and the clearance phase was also slower. Thus, at the end of the experimental period, the fluorescence remaining in the liver was close to 50 % of the maximal value. For NIRBAD-3, the situation was intermediate. The maximal liver load occurred at 1.5 ± 0.2 min, i.e., as fast as that of NIRBAD-1, but the clearance was slower than that of NIRBAD-1, with ≈ 40 % of maximal NIRBAD-3-associated fluorescence still present in the liver at 90 min (Fig. 5A). To quantitatively compare the results in a normalized manner, we calculated the time after injection required to reach the maximum fluorescence intensity in extracorporeal detection (100 %) and during clearance, referred to as NIRBAD clearance time (NCT), needed to reduce fluorescence intensity to 75 % (NCT_{75}), 50 % (NCT_{50}), 25 % (NCT_{25}), and eventually 0 % (NCT_0), only if the latter occurred in less than 90 min (Fig. 5B). All clearance times were shorter for NIRBAD-1 than for the other compounds assayed, including non-vectorized fluorochrome alkynocyanine 718 (Fig. 5B). Accordingly, NCT_{50} for NIRBAD-1 was considered an appropriate parameter for evaluating hepatobiliary secretory function alterations.

3.5. NIRBADs uptake by BA transporters in vitro

The ability to transport NIRBADs by carriers involved in the efficient uptake of BAs by hepatocytes from sinusoidal blood was evaluated in CHO cells stably expressing NTCP, OATP1B1, or OATP1B3. These transporters enhanced NIRBADs uptake, which was inhibited by known substrates, that is, TCA for NTCP and OATP1B1 and rifampicin for OATP1B3. However, the different chemical structures of NIRBADs (Fig. 1A-C) accounted for the different interactions with the assayed BA transporters. OATP1B1 had the lowest ability to transport NIRBAD-2, whereas NIRBAD-1 and NIRBAD-3 transport through this carrier was negligible. OATP1B3 was highly efficient in transporting NIRBAD-1, NIRBAD-2, and NIRBAD-3. However, the latter was predominantly transported by NTCP, which could also transport NIRBAD-1 and NIRBAD-2 (Fig. 6A-C).

3.6. In silico analysis of the interaction between NIRBAD-1 and OATP1B3

To further evaluate the interaction of the most promising probe, NIRBAD-1, with the transporter that most efficiently enhanced the uptake of this compound, OATP1B3, molecular modeling studies were carried out (see detailed information in Supplementary Fig. 3–8). Previous investigations have highlighted the crucial role of the large extracellular region of transmembrane proteins OATP1B1 and OATP1B3 (between H9 and H10) in their transport activity, which is primarily mediated by interacting with their substrates through hydroxyl groups [31–33]. Our results revealed a zone where molecular interactions occur between the extracellular region of the transporter and deoxycholic acid (DCA), used here as a model BA (Fig. 7A). In the substrate pocket formed by several hydrophobic residues, such as Tyr481, Phe501, Leu512, and Tyr517, hydrophobic interactions were established between the steroid backbone of DCA. The hydroxyl groups and the side chain of that BA molecule are exposed to the extracellular space, forming hydrogen bonds with some residues in the microenvironment. In particular, the hydroxyl group at position 12α forms a hydrogen bond with a water molecule, which in turn is bound to Asn477. In addition, the side chain can rotate at different positions and interact with Asn476. The prediction of the interactions between NIRBAD-1 and OATP1B3 transmembrane regions (Fig. 7B) indicated that, similar to DCA, this probe binds inside the binding pocket of the transporter. However, there were some differences. A hydroxyl hydrogen bond was established between position 3 of NIRBAD-1 and Asp239 (Fig. 7B). This interaction cannot occur with OATP1B1 because, in this protein, the amino acid at that position is serine instead of aspartic acid, which may result in NIRBAD-1 being transported by OATP1B3 more efficiently than by OATP1B1, as observed in uptake assays.

3.7. Evaluation of the usefulness of the NCT test in animal models

As a proof-of-concept, the usefulness of the NCT test was assessed in three animal models of impaired hepatobiliary secretory function. In rats treated with phalloidin, used as a model of intrahepatic hepatocellular cholestasis, a substantial decrease in bile flow (-50 %) was induced (data not shown). This was accompanied by delayed elimination of NIR fluorescence from the liver (Fig. 8A). As expected, when administered to mice with complete obstructive cholestasis due to BDL,

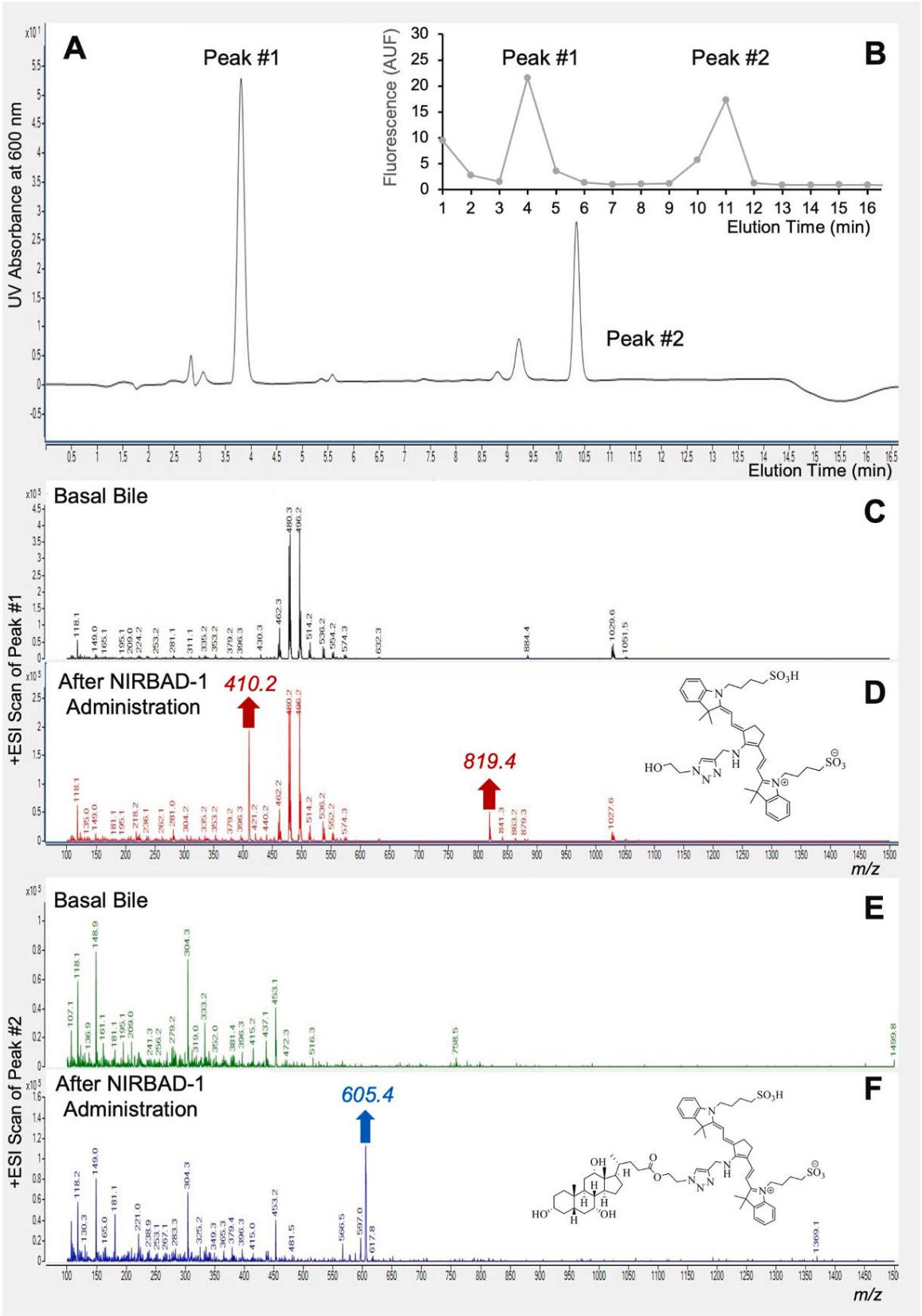

Fig. 4. Separation by HPLC of NIRBAD-1 metabolites in rat bile collected at the time of maximal output of fluorescence after intravenous administration of 1 μmol NIRBAD-1 (A). Detection of two major peaks (#1 and #2) by UV absorbance (B). Fluorescence in 1-min collected fractions during the chromatographic separation. MS/MS analysis of fractions corresponding to elution time of peaks #1 (C and D) and #2 (E and F) after chromatographic separation of bile collected during a 20-min basal period (C and E) or at the time of maximal output of fluorescence after NIRBAD-1 administration (D and F). The insets depict the structures of proposed NIRBAD-1-derived metabolites consistent with mass spectrometric signals absent in basal bile but present in peaks #1 (red arrows) and #2 (blue arrow).

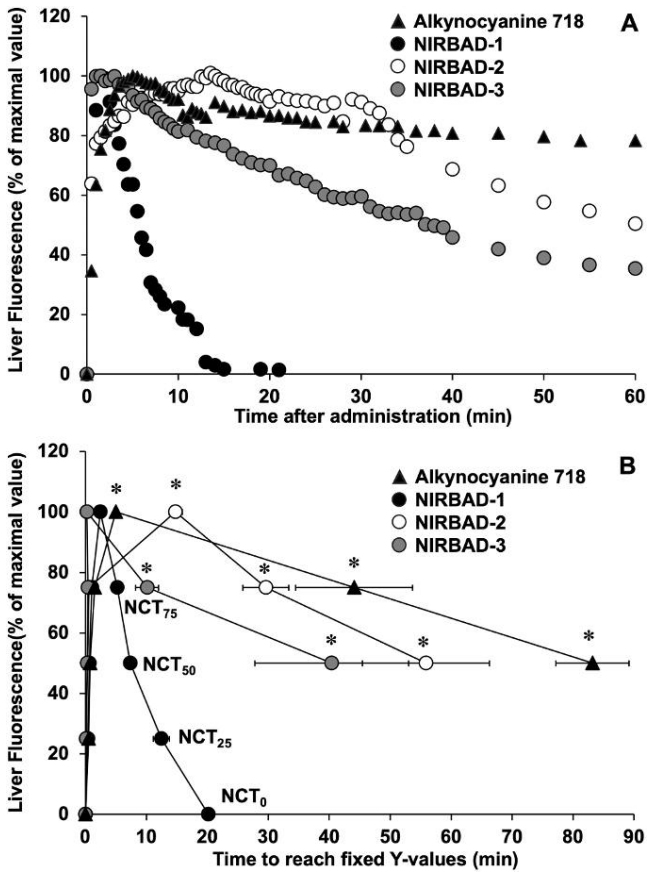

Fig. 5. Real-time recording of liver extracorporeal fluorescence in one representative experiment of each group after intravenous administration of 1 μmol NIRBAD-1, NIRBAD-2, NIRBAD-3, or alkynocyanine 718 to rats (A). Calculation of NIRBAD clearance time (NCT) to reach 75 % (NCT_{75}), 50 % (NCT_{50}), 25 % (NCT_{25}), and 0 % (NCT_0) of the maximal value of fluorescence detected in the liver of each animal (B). Values are mean±SEM ($n \geq 5$). * , $p < 0.05$, compared with NIRBAD-1. Excitation wavelength was 710 nm, whereas fluorescence was recorded using a 785–900 nm LP filter.

NIRBAD-1 rapidly accumulated in the liver and subsequently persisted without significant decay over the experimental period (Fig. 8B). When the dynamics of NIRBAD-1 were analyzed in Mdr2-deficient mice (*Mdr2*$^{-/-}$), used here as a model of impaired bile secretion due to sclerosing cholangitis, both uptake and elimination were reduced compared with wild-type animals (Fig. 8B). Calculation of the NCT values revealed significant differences for NCT_{50} and NCT_{25} between control and phalloidin-treated rats (Fig. 8C). These parameters were also significantly altered in *Mdr2*$^{-/-}$ mice compared to those in wild-type animals (Fig. 8D).

4. Discussion

A novel family of compounds named NIRBADs, obtained by conjugating BA derivatives with fluorochromes using NIR fluorescence, has been recently generated [15]. An essential characteristic of these compounds is their ability to emit light that can penetrate animal tissues. This, combined with their cholephilic behavior, makes them potentially useful tools for studying hepatobiliary function with clear advantages compared to previously used probes, such as ICG, which lack liver specificity [15]. This limitation can be overcome by using NIRBADs owing to the presence of a BA moiety. Functional transport studies revealed that these new probes are recognized as substrates by transporters involved in hepatocyte BA uptake.

Nevertheless, some differences among members of this family of compounds were found, which were consistent with the results of *in vivo* monitoring assays. Thus, although the three NIRBADs assayed were selectively taken up by the liver and subsequently eliminated into bile, based on the dynamics of its transhepatic transit, the best positioned as a helpful probe was NIRBAD-1. Interestingly, consistent with the degree of intracellular lability of the ester bond linking the BA moiety with the fluorochrome during its transit across hepatocytes, NIRBAD-1 undergoes considerable hydrolysis compared to NIRBAD-2 and NIRBAD-3, in which the links occur through stronger bonds (a triazole bond at the C3 position and an amide bond in the side chain, respectively). Hydrolysis of NIRBAD-1 is advantageous because efficient hepatic biotransformation minimizes the risk of long-term permanence of unmodified NIRBAD-1 in the enterohepatic circulation. Indeed, this compound was entirely cleared from the body in less than 24 h (data not shown).

Regarding the uptake studies, the best transporter for NIRBAD-1 was OATP1B3, followed by NTCP. In contrast, NIRBAD-3 was better

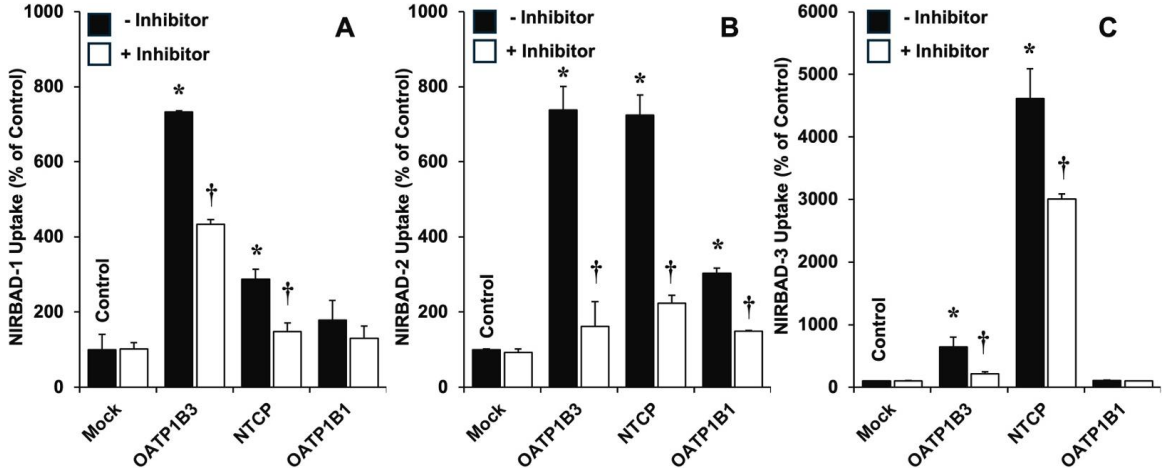

Fig. 6. Transport by carriers involved in bile acid uptake was investigated in CHO-K1 cells stably transduced with an empty vector (Mock), or containing the coding sequence of OATP1B1, OATP1B3, or NTCP. The cells were incubated at 37°C for 15 min with 10 μM NIRBAD-1 (A), NIRBAD-2 (B) or NIRBAD-3 (C) in the absence (black bars) or in the presence (white bars) of 100 μM inhibitor, taurocholic acid (for NTCP and OATP1B1) or rifampicin (for OATP1B3). Uptake was determined by flow cytometry. Arbitrary units of fluorescence (AUF) per cell were normalized in each experiment by considering 100 % the value of AUF in Mock cells incubated in the absence of an inhibitor (Control). Results are mean±SEM from 6 measurements carried out in 3 cultures. * , $p < 0.05$; comparing with Mock cells. †, $p < 0.05$; comparing with values obtained in the absence of an inhibitor.

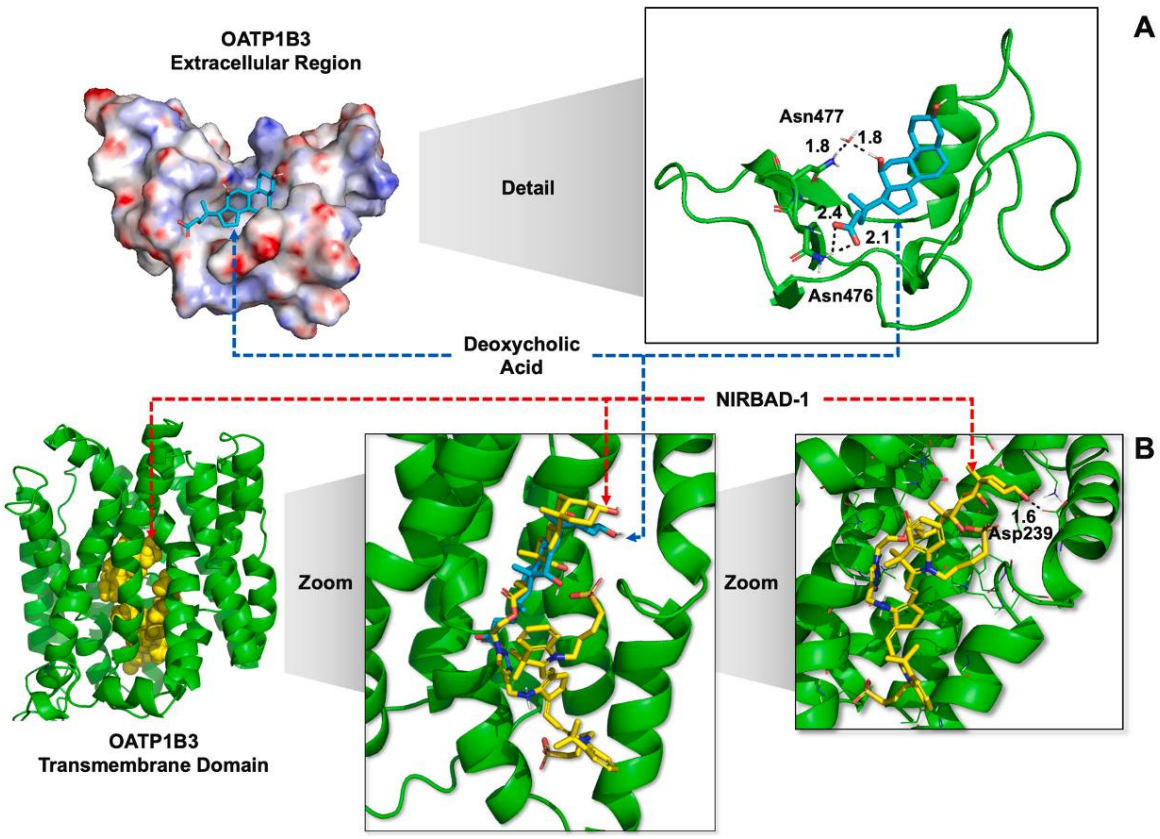

Fig. 7. Predicted binding pose of deoxycholic acid (cyan sticks) in the extracellular region of OATP1B3 showing hydrogen bonds of the bile acid with the residues Asn477 and Asn476 (A). The predicted binding pose of NIRBAD-1 (yellow) shows the transmembrane domain (left, for clarity's sake, some transmembrane domains are omitted) and the binding pocket (right) of OATP1B3, where a hydrogen bond formed with the Asp239 is depicted. The bottom central image shows a comparative representation of the predicted binding poses for NIRBAD-1 (yellow sticks) and deoxycholic acid (cyan sticks) inside the OATP1B3 binding pocket (B).

transported by NTCP followed by OATP1B3. Finally, NIRBAD-2 was equally transported by OATP1B3 and NTCP. OATP1B1 is a poor transporter for these compounds.

Concerning their dynamics in the liver parenchyma, it is noteworthy that, in a healthy liver, there is a zonal distribution of BA uptake transporter expression, which is higher in the pericentral zone than in the periportal zone. This gradient is more marked for OATPs than for NTCP [34]. Moreover, the zonation of BA export pumps goes in the opposite direction, with the bile salt export pump (BSEP) and less markedly multidrug-associated resistance protein 2 (MRP2) being more abundantly expressed in the periportal zone than in the pericentral zone [35]. This is consistent with the differences observed among NIRBADs in intravital studies. NIRBAD-1, which had the fastest uptake and biliary output, was efficiently eliminated from all areas of the liver parenchyma, whereas the slower biliary secretion of NIRBAD-2 and NIRBAD-3 was accompanied by their longer presence in the pericentral zones. It is reasonable to hypothesize that the dissimilar interactions between these compounds and BA transporters are due to their different chemical structures. In this sense, on the one hand, in NIRBAD-2, in which the link to the BA moiety occurs at the 3α position of the steroidal structure, the side chain is free and ends with a negative charge due to the carboxylate. In contrast, NIRBAD-1 and NIRBAD-3 were synthesized by modifying the side chain, leaving the BA steroidal core free. However, there are also notable differences between these two compounds due to the presence of an ester bond in NIRBAD-1 and an amide bond in NIRBAD-3. The difference between a hydrogen bond acceptor or donor can cause a substantial change in their ability to interact with uptake and efflux of transporters involved in BA traffic across hepatocytes.

In silico docking studies revealed that the conformation of the steroid region in NIRBAD-1 closely resembles the steroidal skeleton of natural BAs, accounting for the similar interactions of these compounds with OATP1B3, which are sufficiently robust to establish molecular recognition between the transporter and both ligands. Thus, our results support the concept that OATP1B3 recognizes its substrates primarily via the steroid backbone. Movement through the transporter channel begins with interaction with the extracellular region of the protein. Subsequently, the tail of the molecule (the carboxylic side chain in the case of a natural BA or the fluorescent moiety in the case of NIRBAD-1) follows its path across the plasma membrane towards the intracellular space. Our results agree with previous reports on the impact of the BA structure on the K_M value of this transporter [33,36], suggesting that chemical modifications of the BA side chain, as occurs in NIRBAD-1, are unlikely to dramatically disturb the interactions with OATP1B3, allowing this carrier to recognize NIRBAD-1 as a substrate.

The interaction between efflux ABC pumps involved in the canalicular secretion of BAs and their derivatives (BSEP, MRP2, and BCRP) [37] has not been evaluated here. However, the combination of data from metabolism and dynamics of bile output suggests that they could efficiently export NIRBAD-1. The secretion of NIRBAD-2 and NIRBAD-3 appeared to be less efficient.

As a proof of concept, NIRBAD-1 was administered to animal models with markedly impaired hepatobiliary secretory function. In the complete absence of bile secretion due to BDL [38], once the fluorescent probe accumulated in the liver, the extracorporeal fluorescence was maintained over the experimental period. These results suggest that NIRBAD-1 has marked organ selectivity and that minor reflux from the liver to the blood and elimination by the kidney occur even when biliary output is blocked. Moreover, in phalloidin-induced cholestasis [28], the NCT test clearly visualized impairment in hepatobiliary secretory function. Finally, in mice with cholestasis due to sclerosing cholangitis

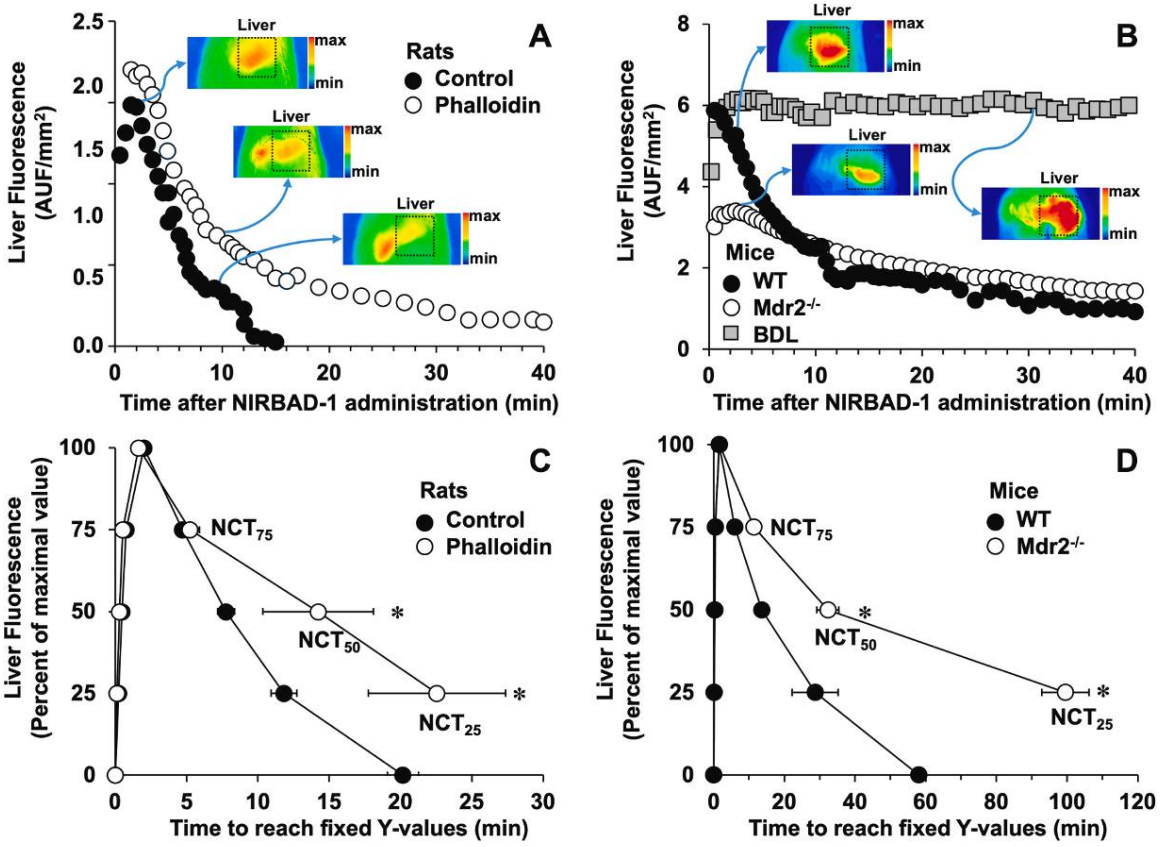

Fig. 8. Usefulness of NIRBAD clearance time (NCT) test in animal models of impaired hepatobiliary secretory function. Hepatocellular cholestasis was induced by phalloidin administration (i.v.; 75 μg/100 g b.w.) in rats (n = 6). Control group included healthy untreated rats (n = 6). *Mdr2*$^{-/-}$ mice (n = 11) were used as a model of sclerosing cholangitis, which was compared with wild-type littermates (n = 6). Obstructive cholestasis was imposed by common bile duct ligation (BDL) for a week in mice (n = 5). Real-time recording of liver extracorporeal fluorescence in one representative experiment of each group after intravenous administration of NIRBAD-1 to rats (A, 1 μmol) or mice (B, 200 nmol). The insets depict characteristic images taken at representative time points (indicated by blue arrows) of each experimental model. Calculation of NCT required to reach 75 % (NCT_{75}), 50 % (NCT_{50}), and 25 % (NCT_{25}) of the maximal value of fluorescence detected in the liver of each animal (C, D). Values are mean±SEM. * , $p < 0.05$, compared with Control or WT groups. Excitation wavelength was 710 nm, whereas fluorescence was recorded using a 785–900 nm LP filter.

[39], dysfunctional secretory machinery was also evidenced by the NCT test. It is worth noting that being a surrogate model of primary sclerosing cholangitis, *Mdr2*$^{-/-}$ mice are one of the best-characterized models of progressive liver injury, inflammation, fibrosis, and ultimately, HCC development that does not rely on the administration of hepatotoxicants [40,41]. The implementation of the NCT test in this clinically relevant mouse model can provide further mechanistic insights into the evolution of the disease in living animals. Moreover, this test could be very useful for monitoring the efficacy of hepatoprotective and anti-fibrogenic therapeutic strategies, which are also reliably tested in *Mdr2*$^{-/-}$ mice [42,43].

In conclusion, these new BA derivatives present appropriate cholephilic characteristics to use them as probes in studies of hepatobiliary functionality by determining the hepatic loading and clearance dynamics of the compounds analyzed by real-time detection of extracorporeal fluorescence. Although further technical adaptations and toxicological studies are required to envisage the translation of the NCT test to clinical practice, this is already a helpful research tool using intact anesthetized laboratory animals to address unanswered questions in the fields of hepatobiliary physiology, pathophysiology, and pharmacology.

Funding information

This study has been funded by the Spanish Ministry of Science and Innovation (Proyectos de Generación de Conocimiento 2022: PID2022-140210OB-I00), Fondo de Investigaciones Sanitarias, Instituto de Salud Carlos III, Spain, co-funded by the European Regional Development Fund/European Social Fund, "Investing in your future" (PI20/00189, PI22/00526 and PI23/00681); CIBERehd (EHD15PI05/2016); "Junta de Castilla y Leon" (SA113P23); AECC Scientific Foundation (2023/2027), Spain; FEEH, Juan Cordoba Fellowship, Grant 2021, University of Salamanca ("Fundación General: Plan TCUE 2015–2017", Plan TCUE (ITR) 2018–2020 (2021) and "Programa de financiación de grupos de investigación. Modalidad C2, 2019–2020"). B. S. de B. received a fellowship from the University of Salamanca co-funded by "Banco Santander." C.C.-L. was supported by a pre-doctoral contract funded by the Ministry of Science and Innovation, Spain (BOE-B-2017–72875). The University of Salamanca supported A.G.T. through the Margarita Salas postdoctoral fellowship program, sponsored by the NextGeneration EU program of the European Union.

CRediT authorship contribution statement

Sanchez de Blas Beatriz: Writing – review & editing, Writing – original draft, Investigation. **Temprano Alvaro G.:** Writing – review & editing, Writing – original draft, Investigation. **Cives-Losada Candela:** Writing – review & editing, Investigation. **Briz Oscar:** Writing – review & editing, Investigation, Funding acquisition. **Lozano Elisa:** Writing – review & editing, Investigation. **Martinez-Chantar Maria L.:** Writing – review & editing, Investigation. **Avila Matias A.:** Writing – review & editing, Investigation. **Mori Mattia:** Writing – review & editing, Investigation. **Ghallab Ahmed:** Writing – review & editing, Investigation.

Hengstler Jan G.: Writing – review & editing, Investigation. **Perez-Melero Concepción:** Writing – review & editing, Investigation. **Bermejo-Gonzalez Francisco A.:** Writing – review & editing, Investigation, Conceptualization. **Monte Maria J.:** Writing – review & editing, Investigation, Funding acquisition. **Romero Marta R.:** Writing – review & editing, Writing – original draft, Investigation, Funding acquisition, Conceptualization. **Marin Jose J.G.:** Writing – review & editing, Writing – original draft, Investigation, Funding acquisition, Conceptualization.

Declaration of Competing Interest

The authors declare that they have no known competing financial interests or personal relationships that could have appeared to influence the work reported in this paper.

Acknowledgments

The authors would like to thank Cesar Raposo for his assistance with mass spectrometry analyses and Dr. Anna M. Lithgow and Samantha Sánchez Curto (NMR Service, NUCLEUS, University of Salamanca) for the NMR spectra done in the Bruker Avance NEO 400 MHz. The authors also thank Emilia Flores for her laboratory technical assistance and Mariar Franco García and Javier Escudero Curto for their secretary work.

Patient consent for publication

Not applicable

Appendix A. Supporting information

Supplementary data associated with this article can be found in the online version at doi:10.1016/j.biopha.2025.118074.

Data availability

Data will be made available on request.

References

[1] B. Sanchez de Blas, A.G. Temprano, J.J.G. Marin, M.R. Romero, Monitoring the hepatobiliary function using image techniques and labeled cholephilic compounds, Explor. Dig. Dis. 2 (2023) 18–33.
[2] F. Holzinger, C.D. Schteingart, H.T. Ton-Nu, S.A. Eming, M.J. Monte, L.R. Hagey, A.F. Hofmann, Fluorescent bile acid derivatives: relationship between chemical structure and hepatic and intestinal transport in the rat, Hepatology 26 (5) (1997) 1263–1271.
[3] S. De Lombaerde, S. Neyt, K. Kersemans, J. Verhoeven, L. Devisscher, H. Van Vlierberghe, C. Vanhove, F. De Vos, Synthesis, in vitro and in vivo evaluation of 3beta-[18F]fluorocholic acid for the detection of drug-induced cholestasis in mice, PLoS One 12 (3) (2017) e0173529.
[4] H. Lambie, A.M. Cook, A.F. Scarsbrook, J.P. Lodge, P.J. Robinson, F.U. Chowdhury, Tc99m-hepatobiliary iminodiacetic acid (HIDA) scintigraphy in clinical practice, Clin. Radio. 66 (11) (2011) 1094–1105.
[5] B.E. Van Beers, J.L. Daire, P. Garteiser, New imaging techniques for liver diseases, J. Hepatol. 62 (3) (2015) 690–700.
[6] S.B. Mondal, S. Gao, N. Zhu, R. Liang, V. Gruev, S. Achilefu, Real-time fluorescence image-guided oncologic surgery, Adv. Cancer Res. 124 (2014) 171–211.
[7] Y. Roggo, P. Chalus, L. Maurer, C. Lema-Martinez, A. Edmond, N. Jent, A review of near infrared spectroscopy and chemometrics in pharmaceutical technologies, J. Pharm. Biomed. Anal. 44 (3) (2007) 683–700.
[8] F.P. Verbeek, J.R. van der Vorst, B.E. Schaafsma, M. Hutteman, B.A. Bonsing, F. W. van Leeuwen, J.V. Frangioni, C.J. van de Velde, R.J. Swijnenburg, A. L. Vahrmeijer, Image-guided hepatopancreatobiliary surgery using near-infrared fluorescent light, J. Hepatobiliary Pancreat. Sci. 19 (6) (2012) 626–637.
[9] K. Purich, J.T. Dang, A. Poonja, W.Y.L. Sun, D. Bigam, D. Birch, S. Karmali, Intraoperative fluorescence imaging with indocyanine green in hepatic resection for malignancy: a systematic review and meta-analysis of diagnostic test accuracy studies, Surg. Endosc. 34 (7) (2020) 2891–2903.
[10] C. Qi, H. Zhang, Y. Chen, S. Su, X. Wang, X. Huang, C. Fang, B. Li, X. Xia, P. He, Effectiveness and safety of indocyanine green fluorescence imaging-guided hepatectomy for liver tumors: a systematic review and first meta-analysis, Photo Photo Ther. 28 (2019) 346–353.
[11] H.K. Dutta, D.N. Rao, D.K. Gupta, Indocyanine green clearance test to evaluate liver function in rat model of extrahepatic biliary atresia, Afr. J. Paediatr. Surg. 15 (1) (2018) 5–9.
[12] C. Schwarz, I. Plass, F. Fitschek, A. Punzengruber, M. Mittlbock, S. Kampf, U. Asenbaum, P. Starlinger, S. Stremitzer, M. Bodingbauer, K. Kaczirek, The value of indocyanine green clearance assessment to predict postoperative liver dysfunction in patients undergoing liver resection, Sci. Rep. 9 (1) (2019) 8421.
[13] T. Namikawa, T. Sato, K. Hanazaki, Recent advances in near-infrared fluorescence-guided imaging surgery using indocyanine green, Surg. Today 45 (12) (2015) 1467–1474.
[14] S.H. Lim, H.T.A. Tan, V.G. Shelat, Comparison of indocyanine green dye fluorescent cholangiography with intra-operative cholangiography in laparoscopic cholecystectomy: a meta-analysis, Surg. Endosc. 35 (4) (2021) 1511–1520.
[15] A.G. Temprano, B. Sanchez de Blas, C. Perez-Melero, R. Espinosa-Escudero, O. Briz, P. Cinca-Fernando, L. LLera, M.J. Monte, F. Bermejo, J.J.G. Marin, M.R. Romero, Synthesis, characterization, and potential usefulness in liver function assessment of novel bile acid derivatives with near-infrared fluorescence (NIRBAD), Bioconjugate Chem. 35 (7) (2024) 971–980.
[16] L.M. Maglova, A.M. Jackson, X.J. Meng, M.W. Carruth, C.D. Schteingart, H.T. Ton-Nu, A.F. Hofmann, S.A. Weinman, Transport characteristics of three fluorescent conjugated bile acid analogs in isolated rat hepatocytes and couplets, Hepatology 22 (2) (1995) 637–647.
[17] M. Alonso-Pena, R. Espinosa-Escudero, E. Herraez, O. Briz, M.L. Cagigal, J. M. Gonzalez-Santiago, A. Ortega-Alonso, C. Fernandez-Rodriguez, L. Bujanda, M. Calvo Sanchez, D.A. D, M.C. Londono, M. Diago, J.C. Fernandez-Checa, C. Garcia-Ruiz, R.J. Andrade, F. Lammert, J. Prieto, J. Crespo, J. Juamperez, A. Diaz-Gonzalez, M.J. Monte, J.J.G. Marin, Beneficial effect of ursodeoxycholic acid in patients with acyl-CoA oxidase 2 (ACOX2) deficiency-associated hypertransaminasemia, Hepatology 76 (5) (2022) 1259–1274.
[18] S. Mita, H. Suzuki, H. Akita, H. Hayashi, R. Onuki, A.F. Hofmann, Y. Sugiyama, Inhibition of bile acid transport across Na+/taurocholate cotransporting polypeptide (SLC10A1) and bile salt export pump (ABCB 11)-coexpressing LLC-PK1 cells by cholestasis-inducing drugs, Drug Metab. Dispos. 34 (9) (2006) 1575–1581.
[19] C. Gui, Y. Miao, L. Thompson, B. Wahlgren, M. Mock, B. Stieger, B. Hagenbuch, Effect of pregnane X receptor ligands on transport mediated by human OATP1B1 and OATP1B3, Eur. J. Pharm. 584 (1) (2008) 57–65.
[20] M. Asensio, E. Herraez, R.I.R. Macias, E. Lozano, L. Munoz-Bellvis, L. Sanchez-Vicente, A. Morente-Carrasco, J.J.G. Marin, O. Briz, Relevance of the organic anion transporting polypeptide 1B3 (OATP1B3) in the personalized pharmacological treatment of hepatocellular carcinoma, Biochem Pharm. 214 (2023) 115681.
[21] J.A. Bell, Y. Cao, J.R. Gunn, T. Day, E. Gallicchio, Z. Zhou, R. Levy and R. Farid. PrimeX and the Schrödinger computational chemistry suite of programs. International Tables for Crystallography F (18.10) (2012) 534-538.
[22] A. Bairoch, R. Apweiler, C.H. Wu, W.C. Barker, B. Boeckmann, S. Ferro, E. Gasteiger, H. Huang, R. Lopez, M. Magrane, M.J. Martin, D.A. Natale, C. O. Donovan, N. Redaschi, L.S. Yeh, The Universal Protein Resource (UniProt), Nucleic Acids Res. 33 (2005). D154-9.
[23] C. UniProt, UniProt: a worldwide hub of protein knowledge, Nucleic Acids Res. 47 (D1) (2019) D506–D515.
[24] G. Jones, P. Willett, R.C. Glen, A.R. Leach, R. Taylor, Development and validation of a genetic algorithm for flexible docking, J. Mol. Biol. 267 (3) (1997) 727–748.
[25] J.A. Maier, C. Martinez, K. Kasavajhala, L. Wickstrom, K.E. Hauser, C. Simmerling, ff14SB: improving the accuracy of protein side chain and backbone parameters from ff99SB, J. Chem. Theory Comput. 11 (8) (2015) 3696–3713.
[26] J. Wang, R.M. Wolf, J.W. Caldwell, P.A. Kollman, D.A. Case, Development and testing of a general amber force field, J. Comput. Chem. 25 (9) (2004) 1157–1174.
[27] M.J. Monte, A.I. Morales, M. Arevalo, I. Alvaro, R.I. Macias, J.J. Marin, Reversible impairment of neonatal hepatobiliary function by maternal cholestasis, Hepatology 23 (5) (1996) 1208–1217.
[28] E. Herraez, R.I. Macias, J. Vazquez-Tato, C. Hierro, M.J. Monte, J.J. Marin, Protective effect of bile acid derivatives in phalloidin-induced rat liver toxicity, Toxicol. Appl. Pharm. 239 (1) (2009) 21–28.
[29] A. Ghallab, D. Gonzalez, E. Strangberg, U. Hofmann, M. Myllys, R. Hassan, Z. Hobloss, L. Brackhagen, B. Begher-Tibbe, J.C. Duda, C. Drenda, F. Kappenberg, J. Reinders, A. Friebel, M. Vucur, M. Turajski, A.L. Seddek, T. Abbas, N. Abdelmageed, S.A.F. Morad, W. Morad, A. Hamdy, W. Albrecht, N. Kittana, M. Assali, N. Vartak, C. van Thriel, A. Sous, P. Nell, M. Villar-Fernandez, C. Cadenas, E. Genc, R. Marchan, T. Luedde, P. Akerblad, J. Mattsson, H. U. Marschall, S. Hoehme, G. Stirnimann, M. Schwab, P. Boor, K. Amann, J. Schmitz, J.H. Brasen, J. Rahnenfuhrer, K. Edlund, S.J. Karpen, B. Simbrunner, T. Reiberger, M. Mandorfer, M. Trauner, P.A. Dawson, E. Lindstrom, J. G. Hengstler, Inhibition of the renal apical sodium dependent bile acid transporter prevents cholemic nephropathy in mice with obstructive cholestasis, J. Hepatol. 80 (2) (2024) 268–281.
[30] A. Ghallab, R. Hassan, U. Hofmann, A. Friebel, Z. Hobloss, L. Brackhagen, B. Begher-Tibbe, M. Myllys, J. Reinders, N. Overbeck, S. Sezgin, S. Zuhlke, A. L. Seddek, W. Murad, T. Brecklinghaus, F. Kappenberg, J. Rahnenfuhrer, D. Gonzalez, C. Goldring, I.M. Copple, R. Marchan, T. Longerich, M. Vucur, T. Luedde, S. Urban, A. Canbay, T. Schreiter, M. Trauner, J.Y. Akakpo, M. Olyaee, S.C. Curry, J.P. Sowa, H. Jaeschke, S. Hoehme, J.G. Hengstler, Interruption of bile acid uptake by hepatocytes after acetaminophen overdose ameliorates hepatotoxicity, J. Hepatol. 77 (1) (2022) 71–83.

[31] S. Choudhuri, C.D. Klaassen, Elucidation of OATP1B1 and 1B3 transporter function using transgenic rodent models and commonly known single nucleotide polymorphisms, Toxicol. Appl. Pharmacol. 399 (2020) 115039.
[32] F. Meier-Abt, Y. Mokrab, K. Mizuguchi, Organic anion transporting polypeptides of the OATP/SLCO superfamily: identification of new members in nonmammalian species, comparative modeling and a potential transport mode, J. Membr. Biol. 208 (3) (2005) 213–227.
[33] M. Roth, A. Obaidat, B. Hagenbuch, OATPs, OATs and OCTs: the organic anion and cation transporters of the SLCO and SLC22A gene superfamilies, Br. J. Pharmacol. 165 (5) (2012) 1260–1287.
[34] W.A. Murphy, A.M. Diehl, M.S. Loop, D. Fu, C.D. Guy, M.F. Abdelmalek, G. S. Karachaliou, N. Sjostedt, S. Neuhoff, P. Honkakoski, K.L.R. Brouwer, Alterations in zonal distribution and plasma membrane localization of hepatocyte bile acid transporters in patients with NAFLD, Hepatol. Commun. 8 (3) (2024).
[35] P.K. Baier, S. Hempel, B. Waldvogel, U. Baumgartner, Zonation of hepatic bile salt transporters, Dig. Dis. Sci. 51 (3) (2006) 587–593.
[36] K. Alam, A. Crowe, X. Wang, P. Zhang, K. Ding, L. Li, W. Yue, Regulation of organic anion transporting polypeptides (OATP) 1B1- and OATP1B3-mediated transport: an updated review in the context of OATP-mediated drug-drug interactions, Int. J. Mol. Sci. 19 (3) (2018).
[37] J.J. Marin, R.I. Macias, O. Briz, J. M. Banales, M. J. Monte, Bile acids in physiology, pathology and pharmacology, Curr. Drug Metab. 17 (1) (2015) 4–29.
[38] A. Symeonidis, E.G. Trams, Morphologic and functional changes in the livers of rats after ligation or excision of the common bile duct, Am. J. Pathol. 33 (1) (1957) 13–27.
[39] C.D. Fuchs, N. Sroda, H. Scharnagl, R. Gupta, W. Minto, T. Stojakovic, J.T. Liles, G. Budas, D. Hollenback, M. Trauner, Non-steroidal FXR agonist cilofexor improves cholestatic liver injury in the Mdr2(-/-) mouse model of sclerosing cholangitis, JHEP Rep. 5 (11) (2023) 100874.
[40] Y. Popov, E. Patsenker, P. Fickert, M. Trauner, D. Schuppan, Mdr2 (Abcb4)-/- mice spontaneously develop severe biliary fibrosis via massive dysregulation of pro- and antifibrogenic genes, J. Hepatol. 43 (6) (2005) 1045–1054.
[41] V. Mariotti, M. Strazzabosco, L. Fabris, D.F. Calvisi, Animal models of biliary injury and altered bile acid metabolism, Biochim Biophys. Acta Mol. Basis Dis. 1864 (4 Pt B) (2018) 1254–1261.
[42] A. Baghdasaryan, T. Claudel, A. Kosters, J. Gumhold, D. Silbert, A. Thuringer, K. Leski, P. Fickert, S.J. Karpen, M. Trauner, Curcumin improves sclerosing cholangitis in Mdr2-/- mice by inhibition of cholangiocyte inflammatory response and portal myofibroblast proliferation, Gut 59 (4) (2010) 521–530.
[43] A. Claveria-Cabello, L. Colyn, I. Uriarte, M.U. Latasa, M. Arechederra, J. M. Herranz, L. Alvarez, J.M. Urman, M.L. Martinez-Chantar, J.M. Banales, B. Sangro, K. Rombouts, J. Oyarzabal, J.J.G. Marin, C. Berasain, M.A. Avila, M. G. Fernandez-Barrena, Dual Pharmacological targeting of HDACs and PDE5 inhibits liver disease progression in a mouse model of biliary inflammation and fibrosis, Cancers 12 (12) (2020).